



# Effectiveness of UAV-Based Remote Sensing Techniques in Determining Lettuce Nitrogen and Water Stresses

S. Bhandari<sup>1</sup>, A. Raheja<sup>2</sup>, M. R. Chaichi<sup>3</sup>, R. L. Green<sup>3</sup>, D. Do<sup>2</sup>, F. H. Pham<sup>2</sup>, M. Ansari<sup>3</sup>, J. G. Wolf<sup>3</sup>, T. M. Sherman<sup>1</sup>, and A. Espinas<sup>4</sup>

<sup>1</sup>Department of Aerospace Engineering; <sup>2</sup>Department of Computer Science; <sup>3</sup>Department of Plant Sciences; <sup>4</sup>Department of Apparel Merchandising and Management  
California State Polytechnic University, Pomona, CA

A paper from the Proceedings of the  
14<sup>th</sup> International Conference on Precision Agriculture  
June 24 – June 27, 2018  
Montreal, Quebec, Canada

**Abstract.** *This paper presents the results of the investigation on the effectiveness of UAV-based remote sensing data in determining lettuce nitrogen and water stresses. Multispectral images of the experimental lettuce plot at Cal Poly Pomona's Spadra farm were collected from a UAV. Different rows of the lettuce plot were subject to different level of water and nitrogen applications. The UAV data were used in the determination of various vegetation indices. Proximal sensors used for ground-truthing included: handheld spectroradiometer, chlorophyll meter, and water potential meter. Relationship between the aerial and proximal sensor data are shown and discussed. Also shown is the relationship between the sensor data and plant height and leaf numbers.*

**Keywords.** *Remote Sensing, Multispectral Data, Hyperspectral Data, NDVI, GNDVI, EVI, MCARI, WBI, Plant Stress, Ground-Truthing, Precision Agriculture.*

---

The authors are solely responsible for the content of this paper, which is not a refereed publication.. Citation of this work should state that it is from the Proceedings of the 14th International Conference on Precision Agriculture. EXAMPLE: Lastname, A. B. & Coauthor, C. D. (2018). Title of paper. In Proceedings of the 14th International Conference on Precision Agriculture (unpaginated, online). Monticello, IL: International Society of Precision Agriculture.

---

## 1. Introduction

Recently, unmanned aerial vehicles (UAVs) have seen increased use for agricultural applications such as crop stress detection, crop monitoring, and yield prediction using remote sensing

techniques. The main advantage of UAV-based remote sensing is the immediate availability of high resolution data. Near infrared (NIR) images obtained using UAV-based remote sensing techniques help determine the crop performances and stresses due to water and fertilizer deficiencies as well as from diseases (Jones et al., 2004; Daughtry et al., 2000; Franke et al., 2008) of a large area in a short amount of time for precision agriculture, which aims to optimize the amount of water, fertilizers, and pesticides using site-specific management of crops (Bricco et al., 1998). Conventional methods of remote sensing use satellites and manned aircraft (Blakeman et al., 2000; Han et al., 2001). However, the satellite images have low resolutions, and have large revisit periods. Also, satellite images are adversely affected by cloud cover. Manned aircraft have been used for aerial imagery and can provide images with better spectral and spatial resolutions. They can also operate under cloud covers and have shorter revisit periods. However, associated cost is very high and turnaround time is long.

UAVs offer several advantages for precision agriculture over satellites and manned aircraft. UAVs are significantly cheaper and simpler than manned aircraft and satellites. They provide high resolution data due to the low altitudes that they can operate at. Also, UAVs can fly during weather conditions that manned aircraft cannot fly at, and thus are able to provide the remote sensing data throughout the crop season (Swain et al., 2007; Hunt et al., 2010).

Despite these potentials, UAVs have not seen widespread use for precision agriculture. At one point, it was estimated that 80% of domestic UAV use in the U. S. would be for precision agriculture. However, though the UAV-based remote sensing technology has made significant progress in recent years, more work is still required to validate the accuracy of the data and using the data for the optimization of irrigation and fertilizer. The remote sensing data are generally able to differentiate the healthy and unhealthy crops. However, the extent to which the crops are stressed has not yet been fully investigated, thereby making it difficult to determine the exact amount of fertilizer and water required for the crop production and increased yield. This has prevented the adoption of the technology by the agriculture industry and farmers. For the effective use by the farmers and service providers on a routine basis, the process of using the remote sensing data for the optimization of water and fertilizer application must be sufficiently validated, and associated cost must be reduced. To be useful in a meaningful way for precision agriculture, the remote sensing data must provide the crop fertilizer and water stresses fairly accurately. This helps reduce the use of water and fertilizer, thereby reducing the cost, conserving water, and reducing the environmental impacts of over-fertilization.

This paper presents the results of the investigation on the effectiveness of UAV-based remote sensing data in determining lettuce nitrogen and water stresses. UAVs equipped with multispectral sensors were flown over the lettuce plot at Cal Poly Pomona's Spadra farm. The paper shows the correlation between remote sensing data, proximal sensor data, and agronomic measurements (leaf numbers and plant height). Our research focus is validating the accuracy of the remote sensing data so that the data can readily be used for precision agriculture. The proximal sensors used for ground-truthing include handheld spectroradiometer, chlorophyll content meter, and water potential meter.

## **Experimental Design**

Figure 1 shows the experimental lettuce plot design. The test plot has total of three replicate rows (*R1*, *R2*, *R3*), with a 4 meter gap between them. The design is a strip-plot design with four nitrogen treatments forming main plots and four irrigation treatments forming subplots. There are three replications and a total of 48 subplots.

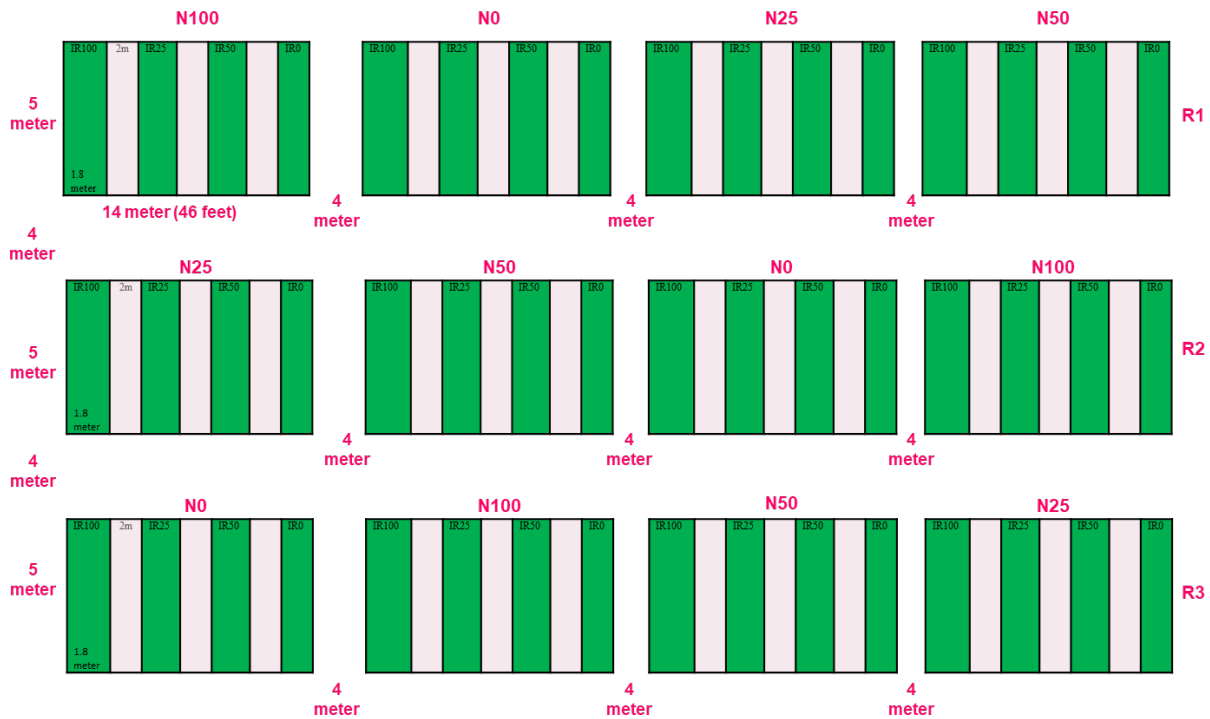


Fig 1. Lettuce plot design.

Each row is 68 meters (223 feet) long, and is divided into four 14 m x 5 m (46 ft x 16.5 ft) plots, with a gap of 4 m between the plots. The large gap between the rows and plots is to avoid the error in data due to nitrogen leaching and water seepage. Each plot is further divided into four 1.8 m x 5 m subplots with a gap of 2 meters between the subplots. The plots are treated with different levels of water application, while keeping the level of nitrogen application the same. For example, the first plot (upper left plot in Figure 1) is treated with 100% nitrogen (N100), while each subplot was treated with a different level of irrigation, i.e., 0% irrigation (IR0), 25% (IR25), 50% (IR50), and 100% irrigation (IR100). The soil nitrogen level was determined prior to beginning the study by sending the samples of the soil to a soil testing lab. The plots were drip irrigated at 0%, 25%, 50%, and 100% of irrigation level that is estimated by the evapotranspiration calculations. Similarly, the nitrogen treatment was slow release nitrogen at 0%, 25%, 50%, and 100% of the nitrogen recommended for lettuce growth after taking into account the existing nitrogen in the soil.

The actual water requirement for the lettuce production was determined using the crop evapotranspiration ( $ET_c$ ), estimated from the potential evapotranspiration ( $ET_o$ ), as given below:

$$ET_c = ET_o \times K_c \quad (1)$$

where  $ET_o$  (in inches) is calculated by the Penman equation with a wind function (CIMIS  $ET_o$ ) (Allen et al., 1998) using the daily data provided by the California Irrigation Management Information System (CIMIS) weather station at Cal Poly Pomona. Studies have shown there is no significant difference between CIMIS  $ET_o$  and Penman–Monteith  $ET_o$ . The coefficient  $K_c$  is the crop coefficient and is defined as the ratio of the crop evapotranspiration rate to the reference evapotranspiration rate. The localized step-wise  $K_c$  of Southern California is used in this study. The amount of water to be applied is then calculated by the following formula:

$$In = \frac{0.623 \times A \times K_c \times ET_o}{IE} \quad (2)$$

where  $In$  is the volume of irrigation water in gallon, 0.623 is the constant,  $A$  is the canopy covered area of the experimental plot surface in sq. ft., and  $IE$  is the irrigation efficiency, which is estimated at 95%. The plot was irrigated on a weekly basis. Prior to irrigation, the soil moisture level was determined using the TDR soil moisture sensor (Al-Jabri et al., 2006), which is shown in Figure

2. This was done to ensure that soil moisture in the different segments of the plot was in agreement with the irrigation level.



Fig 2. TDR soil moisture sensor.

Figure 3 shows the lettuce being grown using the above design. Markers were placed to distinguish the regions of different irrigation and nitrogen application levels. As can be seen in the figure, some plants are more stressed than others.



Fig 3. Lettuce being grown at Cal Poly Pomona's Spadra Farm for the study.

## UAV and Airborne Sensors

The UAV being used for this study is the Lancaster 5 fixed-wing UAV from PrecisionHawk. The UAV, shown in Figure 4, has the empty weight of 5.3 pounds with the maximum takeoff weight of 7.8 pounds. It has a wing span of 4.9 feet and flies at a cruise speed of 40 to 52 feet/sec.



**Fig 4. Lancaster UAV from PrecisionHawk flying over the lettuce plot.**

The UAV can be equipped with different plug-n-play sensors such as a hyperspectral sensor, multispectral sensor, or an RGB camera. The sensors can easily be swapped in the field without reconfiguration. The sensors that are used for this project are a RedEdge multispectral sensor from MicaSense, a BGNIR (Blue-Green-NIR) sensor, Nikon digital camera, and Nano Hyperspec sensor from Headwall Photonics, Inc.

Figure 5 shows the RedEdge sensor. It is a 5-band multispectral sensor. It can capture 5-band spectral data on different wavelengths: blue (475 nm), green (560 nm), red (668 nm), near infrared (840 nm), and red edge (717 nm).



**Fig 5. RedEdge multispectral sensor from MicaSense.**

The BGNIR sensor collects data in the blue, green, and NIR bands. The sensor uses a standard digital camera with a special filter placed inside the camera.

The UAV can also be equipped with a Nano Hyperspec sensor, which is shown in Figure 6. It captures data in 400-1000 nm spectral range, and has 640 spatial bands, 270 spectral bands, and frame rate of 300 Hz. It thus provides much better and detailed measurements than the multispectral sensor. The higher spectral sensitivity of hyperspectral imaging helps detect the stresses at an earlier stage of development (Govendor et al., 2009).



Fig 6. Nano-Hyperspec hyperspectral sensor.

## Proximal Sensors

The proximal sensors used for the validation of the remote sensing data are a handheld spectroradiometer, chlorophyll content meter, and water potential meter (Govender et al., 2018), and are described below.

### Handheld 2 Spectroradiometer

The Handheld 2 Spectroradiometer from ASD is a visible-near infrared (VNIR) hyperspectral sensor, which is shown in Figure 7. It can provide spectral data in 325-1070 nm spectral range, and provides data with an accuracy of  $\pm 1$  nm and a resolution of  $<3$  nm at 700 nm. The spectroradiometer data is used to calculate various vegetation indices including normalized difference vegetation index (NDVI).



Fig 7. Fieldspec Handheld 2 spectroradiometer.

### SPAD 502DL Plus Chlorophyll Meter

The SPAD 502DL Plus chlorophyll meter from Spectrum Technology, shown in Figure 8,

measures chlorophyll content, and can provide information on leaf nitrogen content ((Lindsey et al., 2016; Fox et al., 2008).



Fig 8. SPAD 502D chlorophyll meter.

The chlorophyll meter data for lettuce was compared with the chlorophyll-a and chlorophyll-b contents measured in the lab (Hunt et al., 2014). Figures 9 and 10 show the chlorophyll meter data and actual chlorophyll present in the lettuce leaves. It can be seen that there is a good agreement between the chlorophyll meter data and actual chlorophyll content.

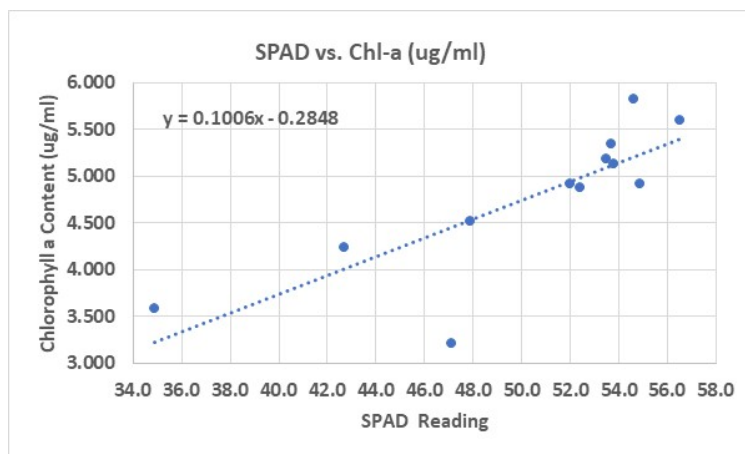


Fig 9. Relationship between SPAD 502 data and chlorophyll-a.

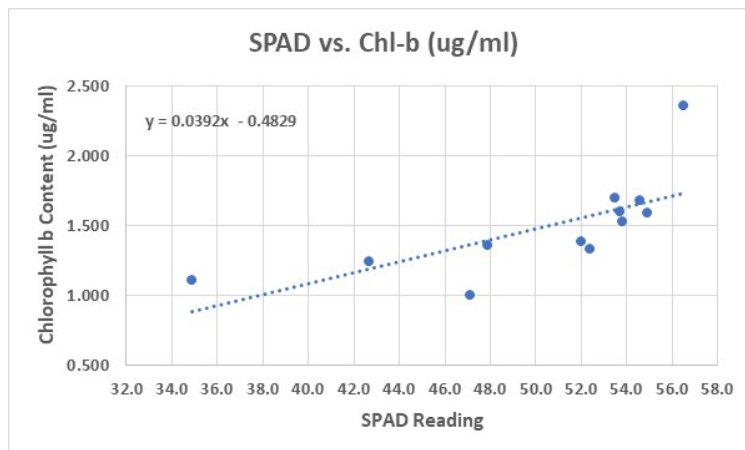


Fig 10. Relationship between SPAD 502 data and chlorophyll-b.

## WPC4 Water Potential Meter

WPC4 water potential meter measures the water potential by determining the relative humidity of the air above a sample in a closed chamber.



Fig 11. WPC4 water potential meter from Decagon.

## Data Collection

The airborne and proximal sensor data were collected on a weekly basis. The remote sensing data from the UAV were collected at close to noon time. The solar noon provides an optimal condition for the remote sensing data as the sunlight is more direct. Handheld spectroradiometer and chlorophyll data were collected and either before or after the data collection from the UAVs were completed. For water potential, leaves were collected from the plants and taken to the Lab in a sealed plastic bag to measure the water potential. It takes several hours to measure the water potential using the water potential meter.

The UAV data were collected from the entire plot each week the data were collected. However, for the proximal sensor data, only a sample of plants were chosen. Each week, two plants from each of the 48 subplots, for a total of 96 plants, were selected. The spectroradiometer data were collected either at the canopy level or the leaf level using the contact probe with the leaf clip. For the chlorophyll, a total of five readings were taken from the five different locations of each leaf and averaged. For the water potential, only one leaf per subplot was chosen.

## Data Processing

The UAV data was processed using the PrecisionMapper software. The cloud based software automatically processes the UAV data into 2D or 3D products as requested by the user. The collected images are orthomosaicked by the software, i.e., the individual raw images are orthorectified and then mosaicked to produce a single image.

The processed images were then converted to a GeoTIFF format, which is an image embedded with geo-referencing information. Quantum GIS (QGIS) software was used to open the GeoTIFF files and create a shapefile, which allows cropping the region containing the plot. After cropping the GeoTIFF file, all of the channels from the GeoTIFF were converted to a 3-D array and saved in a binary format while only the RGB channels were saved into a PNG file. The PNG file allowed for the use of more standard image processing tools. Figure 12 on the left shows the processed raw image of a portion of the lettuce plot from the RedEdge sensor, and the figure on the right

shows the image in the GeoTIFF format.

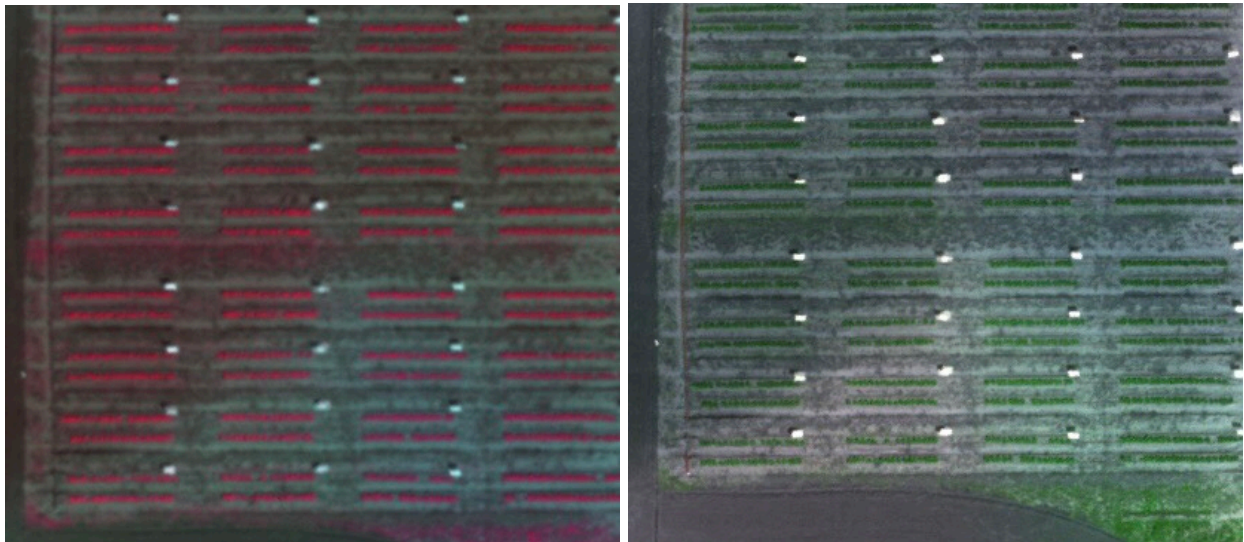


Fig 12. Raw image of the RedEdge sensor data (left) and georeferenced image in GeoTIFF format (right).

Since the rows of lettuce are not oriented in an East to West or North to South fashion, the images were rotated so that bounding boxes around each plant could be more easily drawn. Sloth, a tool for annotating images, was used to create the bounding boxes on the images. The annotations for the bounding boxes were stored in a JavaScript Object Notation (JSON) file format, which was used to crop each individual plant into its own image. It is important to ensure that the order of creating the bounding boxes match with the order of cropping. Otherwise, the cropped image will correspond to the wrong plant (Bhandari et al, 2018).

Using the rotation and annotation information from the JSON file, the same operations were applied to the array so that there was an individual array for each plant. With each of these arrays, the channels were averaged spatially so that there was a single value for each channel.

## Results and Discussion

Using the processed data, several vegetation indices were calculated including normalized difference vegetation index (NDVI), Green NDVI (GNDVI), enhanced NDVI (ENDVI), enhanced vegetation index (EVI), red edge ratio, modified chlorophyll absorption ratio index (MCARI), and dark green color index (DGCI) (Bhandari et al., 2018). For example, the NDVI values are calculated using the following formula:

$$NDVI = \frac{NIR-RED}{NIR+RED} \quad (1)$$

where NIR and RED are reflectances in the NIR and red spectrums. NDVI ratio ranges from -1 to 1. Higher positive NDVI values indicate healthy plants whereas lower values indicate unhealthy plants and negative values indicate unhealthy plants or no vegetation.

Figure 13 shows reflectance plots of two different lettuce plants using the spectroradiometer data. Based on the formula above, the NDVI value for the left plot is 0.92, indicating a very healthy plant whereas the NDVI for the right is 0.56, indicating a less healthy plant.

Similarly, other vegetation indices were calculated (Bhandari et al., 2018). These vegetation indices were compared with chlorophyll meter data, water potential, vegetation indices calculated using the spectroradiometer, and the agronomic measurements that included plant height and leaf numbers. The results shown and discussed below are the best correlations that we could obtain for the various vegetation indices with the proximal sensor data. Some of the best correlations were obtained for a particular day of data collection, while others were obtained for several weeks of data collection.

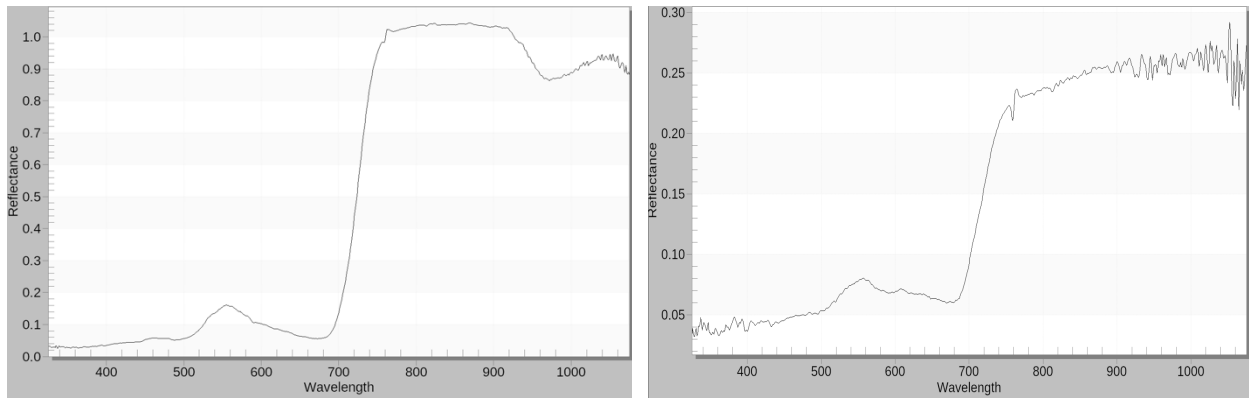


Figure 13. Reflectance plot of a healthy lettuce plant (left) and less healthy plant (right).

Figure 14 shows the relationship between the NDVI obtained using the airborne data from RedEdge sensor and the NDVI obtained using the spectroradiometer data with the Pearson correlation coefficient of 0.55 ( $r = 0.55$ ).

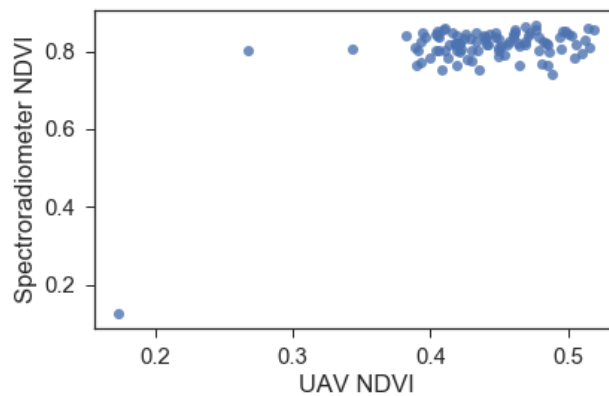


Fig 14. Relationship between UAV NDVI and spectroradiometer NDVI ( $r = 0.55$ ).

Figure 15 shows the UAV NDVI compared with the chlorophyll meter data. A correlation of 0.28 was obtained. The Red Edge ratio had similar correlation with the chlorophyll meter data. However, enhanced vegetation index (EVI) had a lower correlation with the SPAD readings ( $r = 0.2$ ).

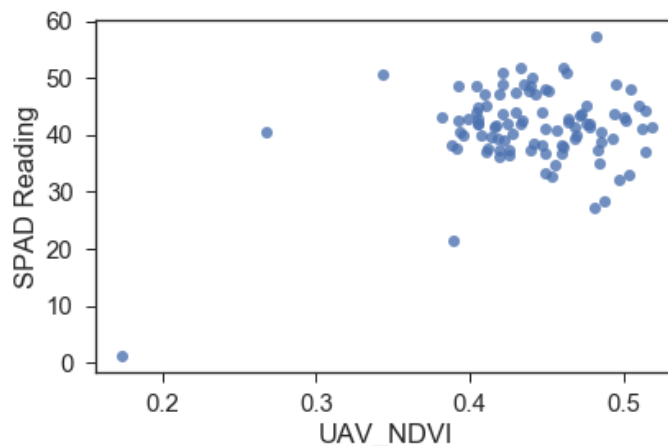


Fig 15. Relationship between SPAD 502 data and UAV NDVI ( $r = 0.28$ ).

However, the modified chlorophyll absorption ratio index (MCARI) showed better correlation with the SPAD readings as shown in Figure 16 with a correlation coefficient of 0.36 ( $r = 0.36$ ).

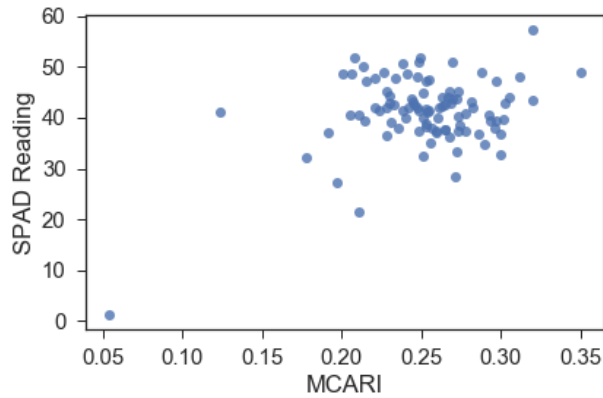


Fig 16. Relationship between MCARI and SPAD readings ( $r = 0.36$ ).

Also, the correlation between Green NDVI (GNDVI) and SPAD readings was better than that between the NDVI and SPAD readings ( $r = 0.35$ ) as seen in Figure 17.

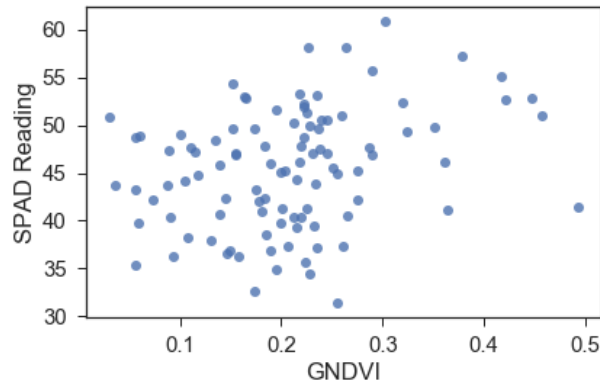


Fig 17. Relationship between GNDVI and SPAD readings ( $r = 0.35$ ).

We also compared the various vegetation indices obtained using the remote sensing and spectroradiometer data with the agronomic measurements (plant height in centimeters and leaf numbers) and total biomass. Figure 18 shows the lettuce height and leaf numbers for different levels of nitrogen application and irrigation. It is seen that both the plant height and leaf numbers are maximum for the 100% irrigation and nitrogen applications. However, it is also worth noting that the plant height for the 100% irrigation and 25% nitrogen levels is same as the height for the 50% irrigation and 50% nitrogen levels. This is helpful in determining the cost-effective application of nitrogen and irrigation for lettuce production using the remote sensing data while also optimizing the yield.

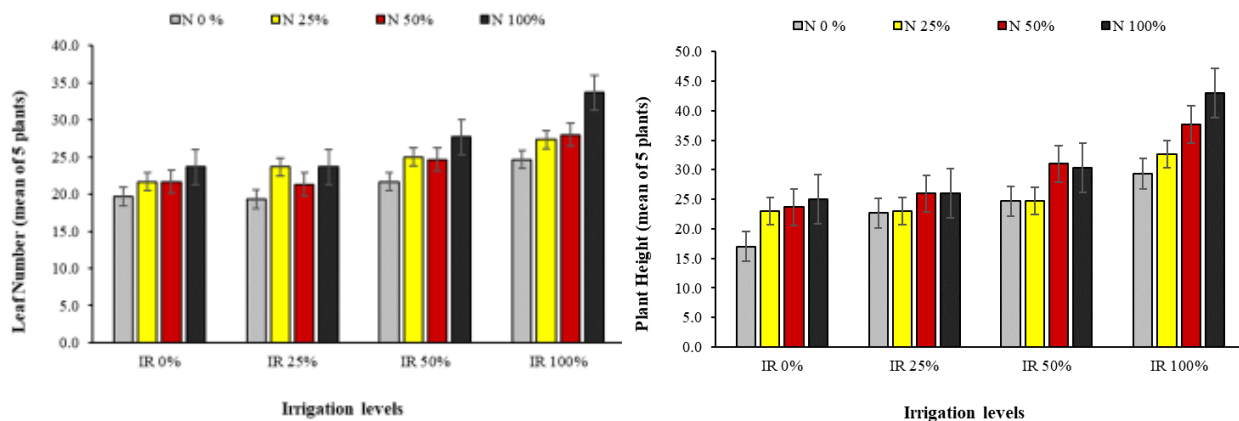


Fig 18. Leaf numbers and plant height vs. irrigation and nitrogen application levels.

Figure 19 shows the total leaf biomass for the different levels of nitrogen application and irrigation. For the total biomass, the leaves were collected from the plants and dried in an oven for 48 hours. The total biomass plot provides the information similar to the information provided by the leaf number plot.

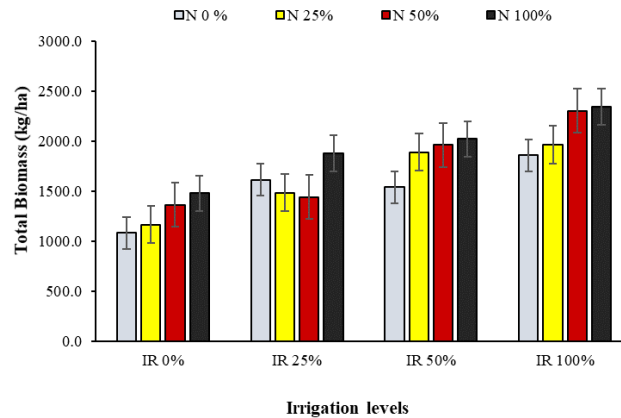


Fig 19. Total leaf biomass for different irrigation and nitrogen application levels.

The relationship between the UAV NDVI and total biomass is shown in Figure 20. A correlation of 0.52 was obtained. EVI had a correlation of 0.45 with the total biomass. All other vegetation indices had lower correlations.

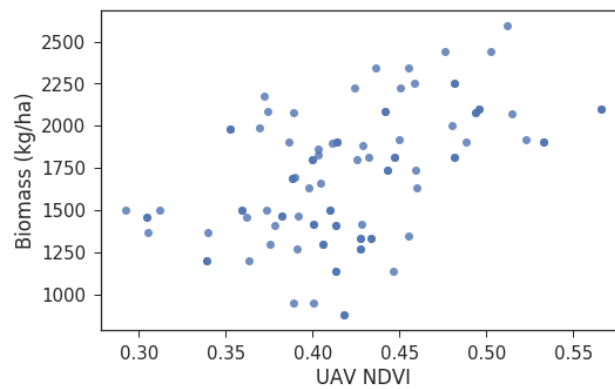


Fig 20. Relationship between total leaf biomass and UAV NDVI ( $r = 0.52$ ).

Figure 21 shows the relationship between the NDVI and average plant height (in centimeters) with a correlation coefficient of 0.46 ( $r = 0.46$ ).

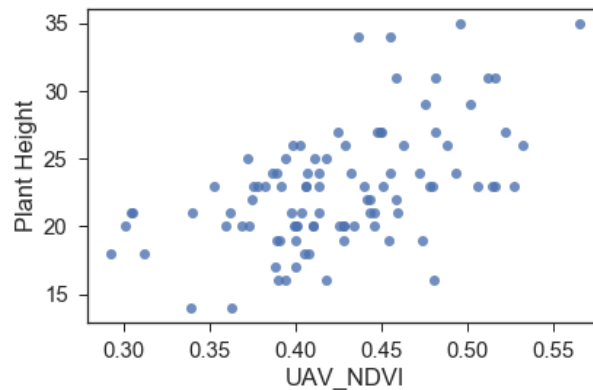


Fig 21. Relationship between NDVI and average plant height ( $r = 0.46$ ).

The Red Edge ratio and EVI had slightly lower correlations ( $r = 0.45$ ) with the plant height whereas the DGCI and GNDVI had about the same correlations of 0.33. For the average leaf count, Red

Edge ratio had the highest correlation ( $r = 0.46$ ) followed by the DGCI ( $r = 0.36$ ) and EVI ( $r = 0.28$ ). The NDVI had the lowest correlation ( $r = 0.24$ ).

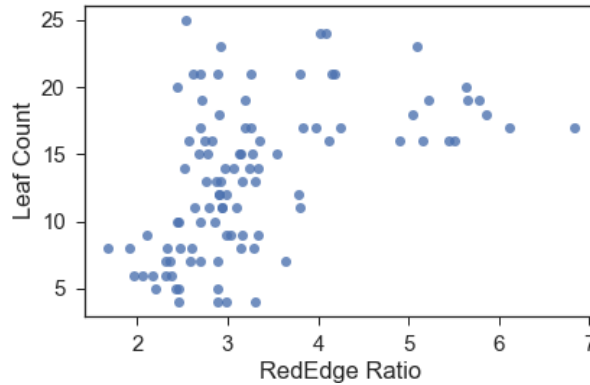


Fig 22. Relationship between Red Edge ratio and average leaf count ( $r = 0.46$ ).

Figure 23 shows the relationship between the EVI and water potential with a correlation coefficient of 0.38. The NDVI and Red Edge ratio had similar correlations with the water potential ( $r = 0.36$ , and  $r = 0.35$ , respectively). However, it should be mentioned that these indices are more indicative of nitrogen content than water.

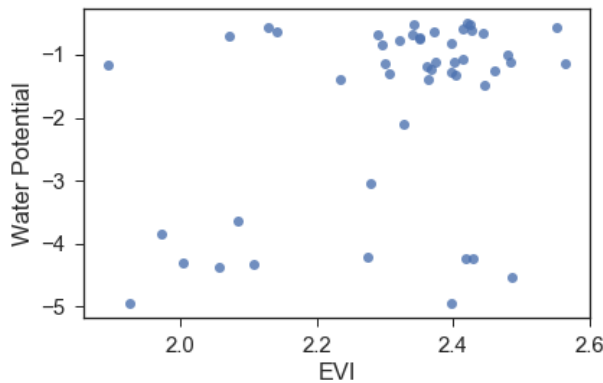


Fig 23. Relationship between EVI and water potential ( $r = 0.38$ ).

The water band index (WBI) was calculated using the spectroradiometer data only. The RedEdge multispectral sensor data cannot be used to calculate the WBI, which is a ratio of the reflectance at 970 nm to the reflectance at 900 nm. The higher the water content in the vegetation canopies, the stronger the absorption at 970 nm relative to the absorption at 900 nm. Figure 24 shows the relationship between the WBI and average leaf count ( $r = 0.62$ ). The average height had similar correlation with the WBI ( $r = 0.59$ ).

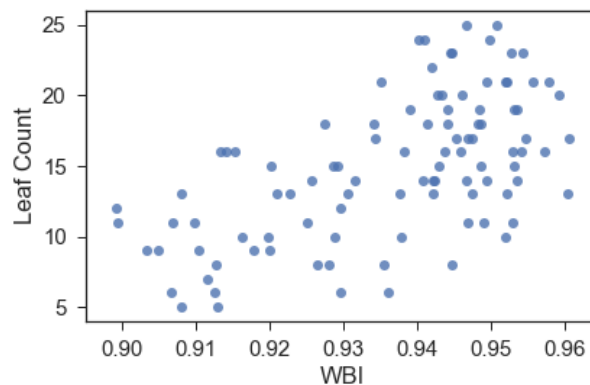


Fig 24. Relationship between WBI and average leaf count ( $r = 0.62$ ).

Figure 25 shows the relationship between the WBI and water potential ( $r = 0.32$ ). The low correlation is probably due to the error in processing the leaves for water potential. This needs to be further investigated.

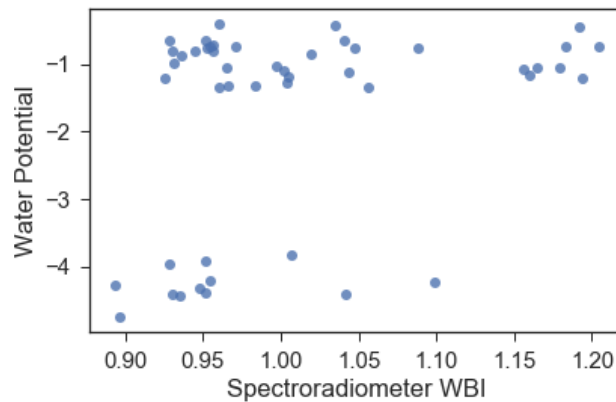


Fig 25. Relationship between WBI and water potential ( $r = 0.32$ ).

The higher correlation between the vegetation indices, leaf count, and plant height indicates that the agronomic measurements may be better indicative of plant health than the information provided by the chlorophyll meter and water potential meter. This also needs to be further investigated.

## Conclusion and Future Work

This paper showed the relationship between the airborne multispectral data and proximal sensor data as well as the agronomic measurements for lettuce plants. Several vegetation indices were calculated using the airborne data and compared with the chlorophyll meter, water potential meter, and handheld spectroradiometer data. The indices were also compared with the plant height and leaf numbers. With the data collected so far, varying degrees of correlations were obtained. The relationship between the UAV NDVI and the spectroradiometer NDVI was the best fit, followed by the relationship between the NDVI and plant height and Red Edge ratio and leaf numbers. Other indices had lower correlation with the ground-truth data. The correlations between the vegetation indices and the chlorophyll was lower than expected. This may be attributed to the fact that the total chlorophyll content depends on both water and nitrogen. The correlations between the water potential and vegetation indices were also less than expected. However, the WBI calculated using the spectroradiometer data had the highest correlations with the plant height and leaf numbers.

From the results obtained so far, it can be concluded that the remote sensing data is generally able to differentiate the healthy and unhealthy plant. However, the remote sensing data is not yet ready to be used for the precision agriculture. The accuracy of the remote sensing data for lettuce needs further validation and investigation.

Future work will involve collecting more airborne and proximal sensor data including hyperspectral data for the different growing seasons of lettuce. The data collection methods will be revisited and improved. This will include determining the best altitude from which to collect the airborne data. Pressure chamber will be used for water potential. We will also measure the leaf area index using a plant canopy analyzer. Since the UAV measures canopy level data, leaf area index is expected to have better correlation with the vegetation indices calculated using the UAV data.

## Acknowledgements

The authors would like to acknowledge the support from California State University's Agriculture Research Institute (ARI). The project is supported by the ARI Grant Numbers 17-04-235 and 18-04-248. We would like to thank Dr. David Still in the Department of Plant Sciences at Cal Poly

Pomona for his valuable inputs, expert opinions, and support of the project. The authors would also like to thank PrecisionHawk for their help with the processing of the airborne data.

## References

- Jones, C., Weckler, P. R., et al. (2004). Estimating water stress in plants using hyperspectral sensing. In Proceedings of ASAE/CSAE Annual International Meeting. Ottawa, Canada.
- Daughtry, C. S. T., Walthall, C. L., et al. (2000). Estimating corn leaf chlorophyll concentration from leaf and canopy reflectance. *Remote Sensing and Environment*, 74(2), 229-239.
- Franke, J., Mewes, T., & Menz, G. (2008). Airborne hyperspectral imaging for the detection of powdery mildew in wheat. In Proceedings of SPIE 7086, Imaging Spectrometry XIII, doi: 10.1117/12.795040.
- Bricco, B., Brown, R. J., et al. (1998). Precision agriculture and the role of remote sensing: a review. *Canadian Journal of Remote Sensing*, 24(3), 315-327.
- Blakeman, R. H., Bryson, R., & Dampney, P. (2000). Assessing crop condition in real-time using high resolution satellite imagery. In Aspects of Applied Biology, Remote Sensing in Agriculture (pp. 163-171), Wellesbourne, UK.
- Han, S., Hedrickson, L., & Ni, B. (2001). Comparison of satellite remote sensing and aerial photography for ability to detect in-season nitrogen stress in corn. In Proceedings of the ASAE Annual Meeting, Sacramento, CA.
- Swain, K. C., Jayasuriya, H. P. W., & Salokhe, V. M. (2007). Suitability of low-altitude remote sensing images for estimating nitrogen treatment variations in rice cropping for precision agriculture adoption. *Journal of Applied Remote Sensing*, 1(1), 013547.
- Hunt, E. R., Hively, W. D., et al. (2010). Acquisition of NIR-green-blue digital photographs from unmanned aircraft for crop monitoring. *Remote Sensing*, 2(1), 290-305.
- Allen, R. G., Pereira, L. S., Raes, D., & Smith, M. (1998). Crop evapotranspiration: guidelines for computing crop water requirements. In Irrigation and Drainage (Paper No. 56). Food and Agriculture Organization of the United Nations, Rome, Italy.
- Al-Jabri, S. A., Lee, J., et al. (2006). A dripper-TDR method for in situ determination of hydraulic conductivity and chemical transport properties of surface soils. *Advances in Water Resources*, 29(2), 239-249.
- Govender, M., Chetty, K. et al. (2008). A comparison of satellite hyperspectral and multispectral remote sensing imagery for improved classification and mapping of vegetation. *Water SA*, 34(2), 147-154.
- Govendor, M., Dye, P. J., et al. (2009). Review of commonly used remote sensing and ground-based technologies to measure plant water stress. *Water SA*, 35(5), 741-752.
- Lindsey, A. J., Steinke, K., et al. (2016). Relationship between DGCI and SPAD values to corn grain yield in the eastern corn belt. *Crop, Forage, and Turf Management*.
- Fox, R. H., & Walthall, C. L. (2008). Crop monitoring technology to assess nitrogen status. Nitrogen in Agricultural Systems, American Society of Agronomy, Agronomy Monograph, 49, 647-674.
- Hunt, E. R., & Daughtry, C. S. T. (2014). Chlorophyll meter calibrations for chlorophyll content using measured and simulated leaf transmittances. *Agronomy Journal*, 106(3), 931-939.
- Bhandari, S., Raheja, A., Chaichi, M., Green, R, Do, D., Ansari, M., et al. (2018). Ground-truthing of UAV-based remote sensing data of citrus plants. SPIE Defense + Commercial Sensing, Proceedings of Autonomous Air and Ground Sensing Systems for Agricultural Optimization and Phenotyping III, Kissimmee, FL.